The role of wall friction in the development, decay and breakage of an air turbulent confined confined vortex

THE ROLE OF WALL FRICTION IN THE DEVELOPMENT, DECAY, AND BREAKAGE OF AN AIR TURBULENT CONFINED VORTEX

Victor Francia[1,2], Luis Martin[2], Andrew E. Bayly[3] Mark J.H. Simmons[1]

[1]*School of Chemical Engineering, University of Birmingham, Birmingham,B15 2TT, United Kingdom.*
[2] *Procter & Gamble R &D, Newcastle Innovation Centre, Newcastle upon Tyne, United Kingdom.*
[3] *Procter & Gamble R &D, Beijing Innovation Centre, Beijing, People 's Republic of China.*

Keywords: vortex development, swirl decay, spray drying, swirling flow, wall friction.

Abstract

Particle processing units such as cyclones swirl spray driers and coaters relay upon complex air swirling patterns to be maintained. Very rarely are there detailed experimental data available directly from production units so designs are often required to be scaled up from experience and computational fluid models of similar pilot designs. A number of effects linked to the operation at a full scale are disregarded: to date, spray drying models neglect the influence that the presence of deposits at the unit walls have in the vortex development, the structure of the turbulent boundary layer or the momentum lost to friction.

This work makes use of ultrasonic anemometry to characterise the swirl decay observed in counter-current spray drying towers across different scales, designs and deposit characteristics. The degree of deposition is found to have a remarkable impact in the development of the flow. The presence of deposits exerts a significant friction, reducing the air axial fluxes of momentum along the cylindrical section of the tower. Three distributions were studied, all resulting in a strong decay of the non-dimensional flux of angular momentum, or swirl intensity, as the vortex rises in the unit. The decay rate is found to be correlated with the distribution and morphology of the deposits. Smooth wall assumptions overestimate the carrier phase swirl and subsequently particle centrifugal inertia by up to one order of magnitude. They also fail to reproduce the axial reversion zone that develops at the vortex core for lower operating swirl intensities. The balance between the initial swirl intensity and that surviving at the top appears to be a critical factor determining the recirculation patterns observed in the cylindrical section.

Introduction

Swirling patterns are introduced in multi-phase systems due to their ability to enhance heat and mass transfer rates. The evolution of the flow in open pipes has focused most of the attention in recent decades. The role of swirl intensity, the dependency of the decay rate with Reynolds, the field anisotropy, or the attenuation of the swirling motion and the turbulence caused by the presence of a particle phase are some of the characteristics more commonly investigated.

Swirl intensity and Reynolds play the most important role in the development of the velocity patterns. As described by Maddahian (2011) they have a profound impact in the generation of radial pressure gradients and the configuration of the turbulent boundary layer in force and free vortexes.

The structure of the turbulent boundary layer however may also be disrupted by the friction caused by the wall roughness whenever significant deposits are present at the wall. Alternative definitions of the logarithmic law of the wall aim at describing the impact brought by a rough wall to simple systems (Jimenez 2000). All are of a semi-empirical nature and require values of friction velocity or the wall shear stress to be determined experimentally. Comprehensive experimental works for specific units, such as those presented for the carrier phase by Kioth (1991) or multi-phase systems by Sommerfeld & Qui (1993), Pruvost (2000) or Zhou (2000) allow providing a detailed description of velocity distributions at the near wall region. Proposed wall functions for smooth or rough walls may be implemented as a wall boundary condition for numerical models, such as, for instance in the simulation of the swirl decay in cyclones (Kaya et al 2011). A full model however shall require enough information on the relation between the swirl decay rate and the wall conditions, and how those may relate to the parameters in the wall function, such as roughness height. In addition, depending on the vortex type, the applicability of wall functions themselves remains as an issue for high swirl intensity systems (Jakirlic et al 2002).

The use of high swirl intensities in air particle-laden fields in particular presents the drawback of promoting the interaction between the particles and the wall. The efficiency of systems such as cyclones, spray driers or coaters may suffer the most from it. They can generate a great deal of wall deposition whenever the balance between the centrifugal force and the mechanical properties of airborne particles favours so. Counter-current spray drying towers are known to be specially prompted to it as they carry semi dried droplets within a high swirling turbulent air vortex (Hassall 2011).

Computational modelling of such highly complex systems is not a trivial matter. Most three dimensional models of large

industrial units reduce the complexity arising from wall effects and in the sake of simplicity assume standard smooth walls as the boundary conditions. However, the lack of a systematic set of data across production scales has so far prevented the evaluation of this assumption. Historically, the experimental data is gathered in relatively clean laboratory or pilot scale systems. Among others, the potential effects of wall friction in the vortex energy, and how that might impact the overall development of the flow filed, remains unknown.

Tower designs are also known to vary significantly and small units cannot always replicate the range seen in production, in terms of operating swirl intensities, aspect ratio or wall conditions. Should there be important wall effects; the available scale up rules would need to be reconsidered.

This work aims at breaching such an experimental gap and provides evidences of the wall friction observed in a range of real production units. The impact that deposits introduce in the development of a confined air vortex has been investigated and it is presented along the velocity data obtained in the cylindrical section of three counter current spray drying towers at variable deposition and scale.

Nomenclature

A	Cross sectional area (m^2)
D	Diameter (m)
H	Distance from air inlets to vortex finder (m).
M	Total mass flow rate (kg s^{-1})
R	Radius (m)
S	Swirl number
U	Air velocity (m s^{-1})
V	Volume (m^3)
d	Diameter of the vortex finder (m)
r	Coordinate in the radial direction (m)
u	Velocity fluctuation (m s^{-1})
x	Deposit thickness (m)
z	Coordinate in the axial direction (m).

Greek letters

Ω	Swirl intensity
α	Pre-exponential factor of decay.
β	Exponential rate of decay
θ	Coordinate in the tangential direction (rad)
φ	Alignment to the axial direction (rad).
Υ	Alignment to the radial direction (rad).
ρ	Density (kg m^{-3})
υ	Dynamic viscosity (m^2 s^{-1})
τ	Shear stress (kg m^{-1} s^{-2})

Subscripts

c	At the cylinder.
i	At the air inlets.
m	Mean at the cross section for axial component.
$wall$	At the wall.

Swirl decay. Theoretical background

The decay of an air swirling flow responds to the presence of tangential friction at the wall. Different parameters have been described to quantify this effect (Kreith & Sonju 1965). The non-dimensional angular momentum flux seems to bear the most physical meaning. It arises from the relation between the flux of angular momentum and the wall tangential shear stress and may be derived from the transport equations expressed in polar coordinates. Starting from the Reynolds averaged equation, the tangential wall shear stress (Steenbergen & Voskamp 1998) for a stationary axis symmetric and incompressible vortex reads

$$\tau_{\theta,w(z)} = \frac{\rho}{R^2}\int_0^R r^2 \frac{\partial}{\partial z}\left(\overline{U}_\theta \overline{U}_z + \overline{u_\theta u_z} - \upsilon \frac{\partial \overline{U}_z}{\partial z}\right) dr \quad (1)$$

Where an over head bar indicates time averaging. The last right hand side terms are related to the contribution of turbulent and viscous shear stresses to the transport, which can both be neglected. The evolution of the wall shear stress can then made non dimensional by normalizing the velocities with the mean axial velocity, U_m, in (2).

$$\frac{\tau_{\theta,w(z)}}{\rho \overline{U}_m^2} = \frac{\partial}{\partial z}\int_0^R \frac{\overline{U}_z \overline{U}_\theta}{\overline{U}_m^2 R^2} r^2 . dr \quad (2)$$

This expression may be rewritten as function of the evolution of the non-dimensional flux of angular momentum, known as swirl intensity in (3) (Kioth 1991)

$$\Omega_{(z)} = 2\pi\rho \int_0^R \frac{\overline{U}_z \overline{U}_\theta}{\rho \pi \overline{U}_m^2 R^3} r^2 . dr \quad (3)$$

$$\frac{4\tau_{\theta,wall}}{\rho \overline{U}_m^2} = \frac{d\Omega}{d(z/2R)} \quad (4)$$

As elaborated by Kioth (1991), an exponential decay of Ω along z/D may be only expected from (4) for very low values of Ω, where the relation between shear tress and Ω may be proportional. A piecewise linear relation was proposed for regions above. Nevertheless, the exponential decay in (6) is commonly reported in experimental studies of free developing swirling flows.

$$\Omega_{(z)} = \alpha e^{\beta} \quad (5)$$

In addition, experimental observations and numerical models both, show an inverse relation between the decay rate, β, and Reynolds for smooth cylinders. Little data however is available for the evolution over rough walls, and the range of most studies limits to those of more interest for the flows developed along open pipes, seldom above 1. Alternative definitions of swirl numbers include the ratio of the angular momentum flow to the axial flux of axial momentum divided a reference radius (Guo et al 2001) or the ratio of tangential to total momentum flux based in the bulk mean axial velocity (Cheng & Dhir 1994) given below

$$S = 2\pi\rho \int_0^R \frac{\overline{U}_z \overline{U}_\theta}{\rho \pi \overline{U}_m^2 R^2} r . dr \quad (6)$$

The latter is a convenient measure of the energy carried by the tangential motion in systems of constant D. However, depending on the system it bears a more difficult interpretation. It shows a disadvantage in the study of confined units such as cyclones or swirl towers where the flow is subject to an exit contraction, causing a rapid increase in velocity and a large pressure drop.

As described in figure 1, a counter-current tower generates the swirling motion through a series of inlets directed towards the bottom conical section with a certain tangential component to its velocity. This produces an accelerating vortex upwards into the main body and in this way, a high initial Ω can be achieved at the inlets level, ranging from 0.1 to 10. The air vortex then develops axially in a confined cylindrical section, up to *10 D* and is forced to exit through a contraction at the top. Consequently, free development of the vortex should then not be assumed, and significant axial recirculation may occur. Compressibility effects however may be neglected for the velocity ranges generated.

In this work, the swirl intensity Ω will be estimated making use of experimental velocity profiles. These are available at one or two opposite tangential locations for each axial cross section, due to the presence of consistent field asymmetries. Measurements are not available in a range of positions close to the wall and for some cases, at the centre due to the limitation that the largest scales pose on the experimental procedure. This makes an extrapolation assumption necessary. Centre values are assumed as that of the last known position for axial velocities and zero for the tangential component. Three values are then computed to provide a best estimate of Ω and a certain range in within the actual value lies. U_z and U_θ are extrapolated as follows:

Under-estimation Ω_- : Linear interpolation from the last known position to the wall where all velocities are zero.

Over-estimation Ω_+ : Linear extrapolation from the last two known positions up to the wall.

Best estimate Ω_o : Linear extrapolation from the last two known positions to a boundary from which they follow a logarithmic decay to zero at the wall. The boundary is such that it minimizes the error of the computed axial mass flow for each individual measured radial profile.

Data obtained at previous works by means of particle image velocimetry (Hassall 2011) indicated that in these units, velocities do not start decaying sharply close to the wall up to locations above *0.98 R* for at least the tangential component. As a consequence, the use of Ω_- is expected to yield much greater errors in the integration of the axial mass rate, in particular for the cases B & C defined later, where a large extrapolated range is required. The mass rate errors for Ω_o are kept below 0.1 % with the exception of strongly asymmetrical sections where errors go up to 4 % in scale I or II and up to 13% in the top end of scale III.

Experimental Methodology

Instrumentation

Air velocity magnitude and direction are measured with a Horizontal Symmetry 50 Solent Sonic Anemometer. It comprises of a single metal frame axis and three independent pairs of ultrasonic transducers arranged in a fork-type head frame, designed specifically to minimize aerodynamic disruption. Measurements are taken for 60s with measuring frequencies from 20 to 50Hz. 45 to 240 individual locations cover the cylindrical section. The fork-like head comprising the transducers is placed in each position by fixing the anemometer to a unit door engineered to be assembled around its frame, see figure 2. Accessing positions where the frame length is shorter than required is achieved by fitting an extension bar to the back end. In such cases, measurements with and without the extension provide evidence of no significant disruption to the flow.

Units scale and design

Figure 1 outlines a typical counter current swirl tower. The air delivery system consists on a series of fans operated at ambient conditions. The fan speeds are set manually and their relative head is adjusted to maintain a target inlet mass rate and a constant exit pressure. All data were gathered in the absence of airborne particles. The injection of non-dimensional flux of angular momentum Ω_i is estimated from (7)

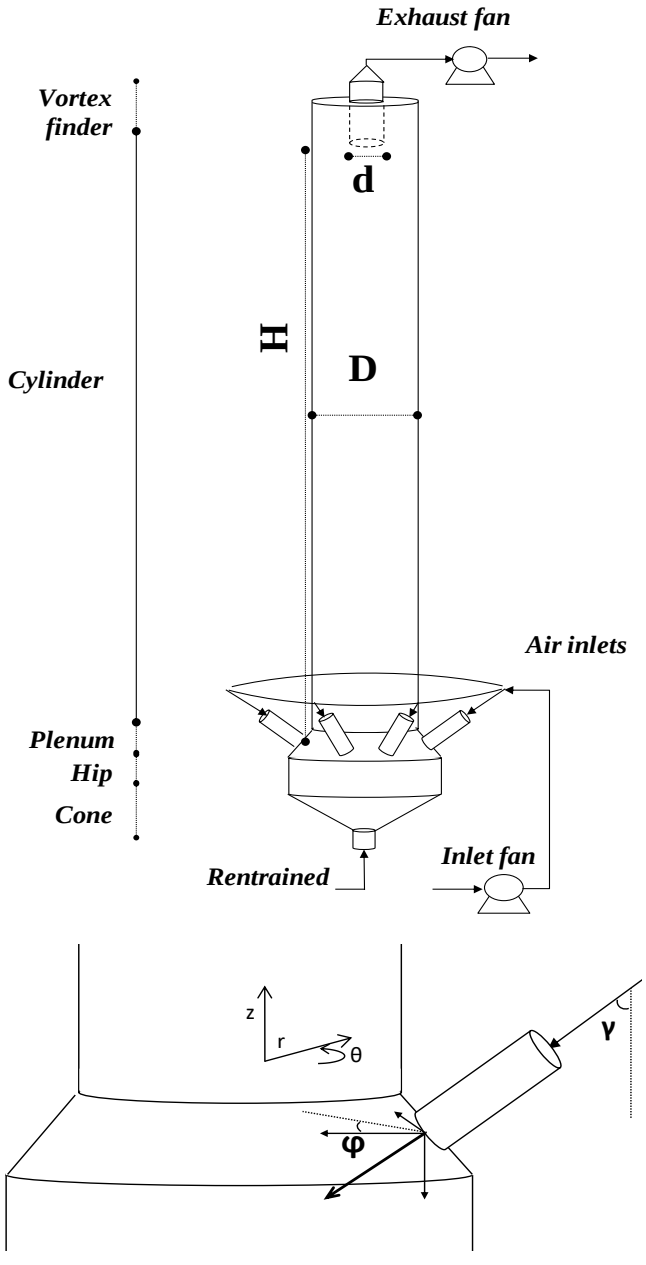

Figure 1: Outline of a counter current spray drying tower including the air inlets alignment details.

Scale	SCALE AND GEOMETRY				Re x 10^{-3}				
	Volume ratio	Aspect ratio		Air inlets	$D\ U_m / \upsilon$				
	$V / V_{Scale\ I}$	H / D	d / D	Ω_i	*Re I*	*Re II*	*Re III*	*Re IV*	*Re V*
I	1	11.8	0.29	5.1	80 - 90	102	120 - 123	180 - 185	-
II	16.1	3.0	0.39	3.4	-	-	-	-	570
III	27.6	2.9	0.31	7.7	-	-	-	-	420

Table 1: Geometry, design parameters and operating Re of experiments conducted in scales I, II & III

$$\Omega_i = \frac{M_i U_{i,\theta} R_i}{M_C U_m R_c} = \frac{M_i}{M_C}\frac{A_C}{A_i}\frac{R_i}{R_c} \cdot \sin\varphi \sin\gamma \qquad (7)$$

The injector alignment angles φ and γ to the radial and axial direction are kept constant between scales and determine the tangential component to the inlet velocity. The ratio between the mass rates through the inlet section Mi and the cylinder M_C is owed to air entrainment from the powder exit at the bottom end of the cone. It is considered constant and as a 5% in mass according to historical numerical simulations. Finally, the ratio between the radius at the inlet R_i and the cylinder R_C sections and the total areas of both A_i and A_C account for the impact of the tower geometry. As a result, each unit operates at a given initial swirl intensity Ω_i exclusive function of the design. Its evolution along the axial direction in the cylindrical section will be related to the history of the tangential wall shear stress experienced by the vortex, described for a simplified system in (1).

Three counter-current spray drying towers of different scales and aspect ratio were investigated. Their relative size ratios, design and operation parameters are given in Table 1

Error sources and corrections

Extensive literature is available covering the sources of error of ultrasonic anemometry (Probst & Cardenas 2010, Cuerva et al 2000, 2003). Those which are a consequence of the unit design and its disruption to the flow field are minimized by the selection and operation of the instrumentation (Walker 2005) and by the appropriate use of correction algorithms (Wilczaki et al 2001). Others are related to the effect that unsteady and non-uniform velocity fields across the sonic path have in the propagation of the wave pulse. These can be minimized here by the orientation of the instrument versus the air vortex, and are estimated as a function of the Mach number (Franchini et al 2007).

The instrument accuracy, established in wind tunnel calibrations, is reported as 1% RMS in speed and 1° in direction. However, the methodology described here differs substantially from most applications within methodological research and in particular the aerodynamic disruption caused to the field needs to be quantified. The instrument is not aligned for the least disruptive orientation versus the streamlines at each location, but at a fix position versus the unit: the head is aligned with the cylinder vertical axis.

The aerodynamic disruption caused will be proportional to the Mach number and errors may be influenced by the turbulence energy (Nakai & Shimoyama 2012). The uncertainty in the measurement will then vary from one location to another depending on the local turbulence and the direction of the mean streamline. Internal instrument calibrations do not replicate these phenomena and so the error range provided here has been obtained from a separate error analysis. It gives a conservative estimate for the uncertainty owed to aerodynamic disruption, error in position and alignment and large time scale variability. Detailed discussion of the experimental methodology, its sources of error and data correction is available under other related works. Special attention is given to the use of the internal calibrations and correction of misalignments.

The use of calibration function is enabled. Mathematical singularities are known to be associated to the use of such correction functions in narrow designs of thee dimensional arrangements of transducers (Cuerva et al 2004). Such effects are indeed identified in this system but introduce no significant error as long as the attack angles fall below those recommended by the manufacturer.

Instrument alignments however need to be accounted for carefully to express the measured velocity in a polar coordinate system referred to the unit. This is achieved by performing three axis gyrations using the real alignments to the cylinder axis and horizontal plane, and alignment between the fitting inspection door and true radial axis of the cylinder. The latter is a common issue in the large units

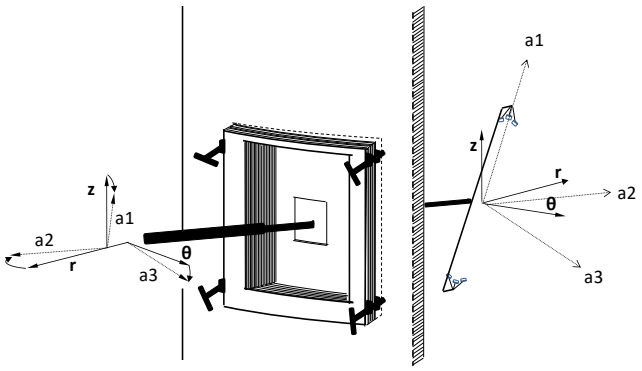

Figure 2: Sketch of the anemometer and door ensemble. Misalignments between the door and the inner wall lead to a deviation between *z* & *a1* and *r* & *a2*. The frame rotation along axis a2 leads to a deviation between *θ* & *a3*.

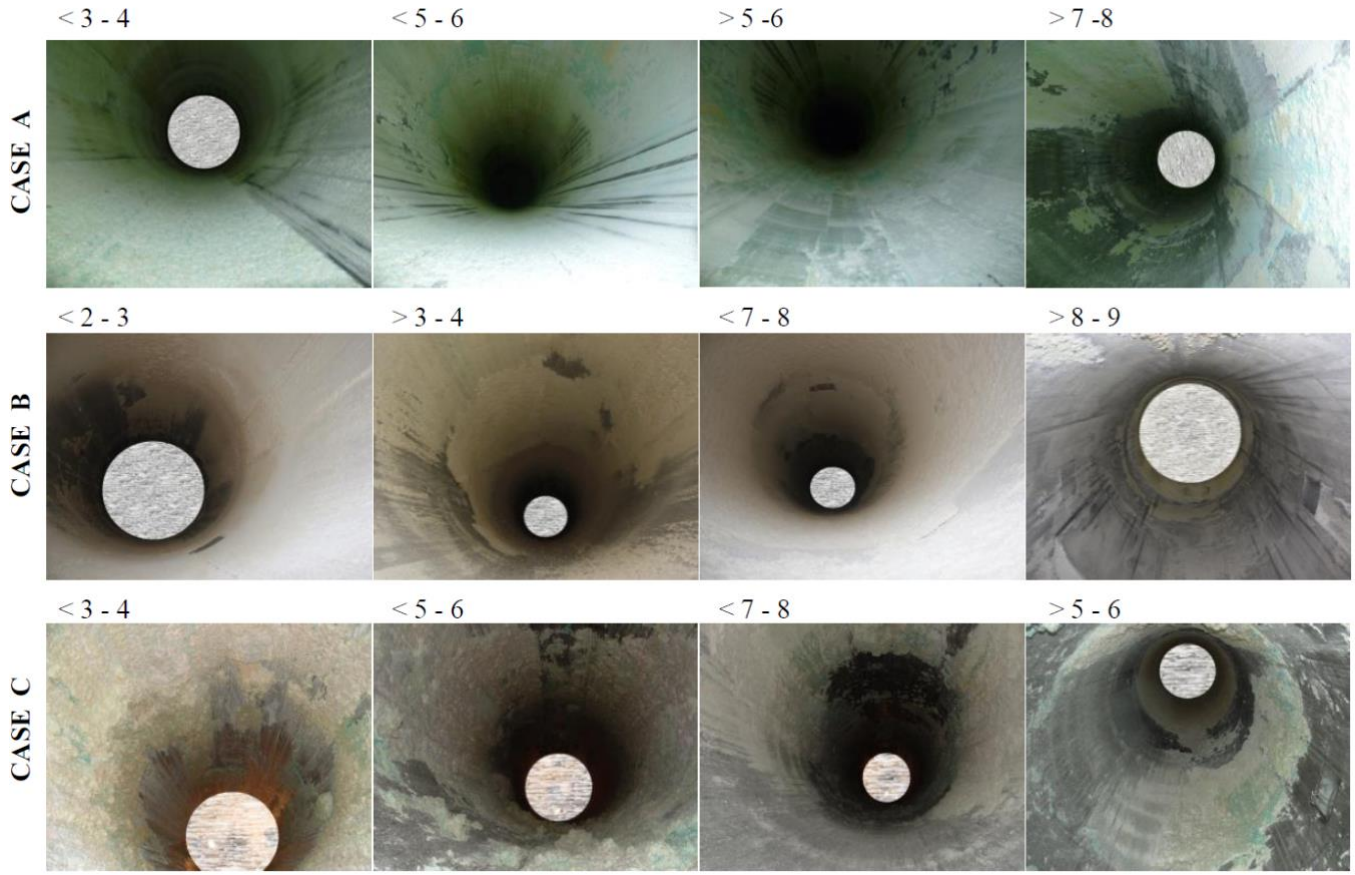

Figure 3: Scale I. Light case A, standard case B and heavy, case B deposits. Axial distribution of deposits. Numbers indicate the orientation and approximate range of axial distances covered in z/D. Nozzles and/or instrumentation in the pictures has been pixilated artificially to protect intellectual property.

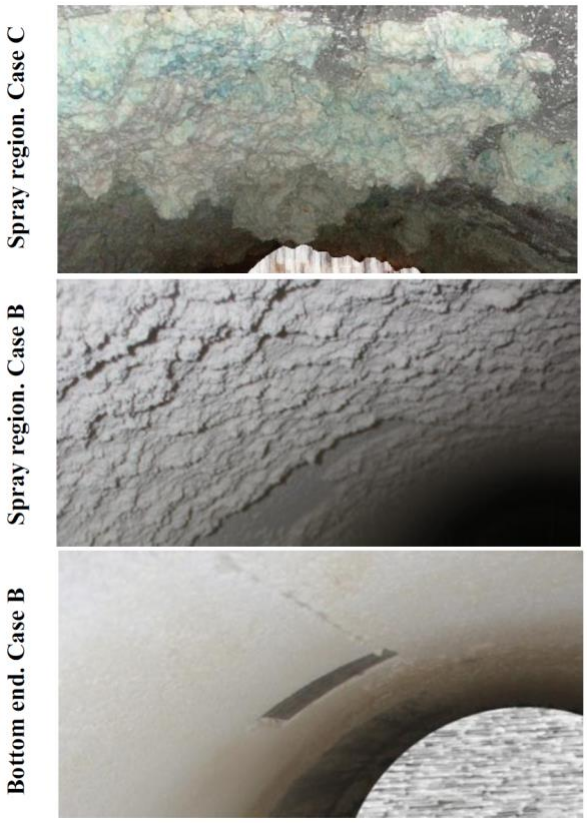

Figure 4: Details of the wall roughness. Cases B & C.

	Location		Coverage		Thickness	
	from	**to**	**from**	**to**	**from**	**to**
	z / D		***% of area***		***x / R . 10²***	
Case A	Cone		100		< 1	
	0.0	7.1				
	7.1	10.6	0	40	0	< 1
Case B	Cone		100		< 1	
	0.0	1.8	15	30	0	< 1
	1.8	2.4	100		< 1	
	2.4	5.7	40	70	0	< 1
	5.7	**7.1**	100		1 – 2	
	7.1	8.1			0 - 1	
	8.2	10.6	Metal			
Case C	Cone		Metal			
	0.0	2.4	5	10	0	< 2
	2.4	**5.7**	100		1 - 2	3 – 5
	5.7	7.1	50	75	0	< 2
	7.1	8.1	10	15		
	8.1	10.6	100			< 1

Table 2: Estimates of deposit coverage and thickness.

where a deviation between the door and the inner wall arises from the building tolerances and the leveling of the door anchoring mechanism, see figure 2. This misalignment translates into a deviation between the HS-50 axis frame and the true radial direction that can lead to large errors in radial position for central locations. It all renders an artificial transfer between the measured tangential and radial components and a high relative error for the latter.

The measured velocities are corrected for all the effects mentioned above and time-averaged fields are then expressed in a polar coordinate system referred to the cylindrical section. Turbulent kinetic energy and Reynolds stresses can then be obtained from the analysis of the statistics of velocity fluctuations.

Wall conditions

Deposits in a counter current spray drying tower occur in bands along the cylinder axis, and are preferentially located in the nozzle/s regions, marked as bold in Table 2. Here, high momentum wet sprays project onto the wall and build up significant layers of product. Figure 3 & 4 illustrate the distribution and morphology of the deposits for the three different scenarios investigated in the scale I, named cases A, B & C, representing conditions of light, standard and heavy wall deposition respectively.

Lower regions in the unit present deposits which are often much highly compacted due to being subject to a faster drying kinetics, and much stronger erosion owed to high air tangential velocities. At higher levels, wet and low density layers are constantly being formed and eroded, leading to a reasonable stable thickness, presumably due to the equilibrium between erosion and deposition processes.

Results and discussion

Vortex development

Figures 5 & 6 show the evolution of the tangential and axial velocity profiles for the smallest unit in table 1, scale

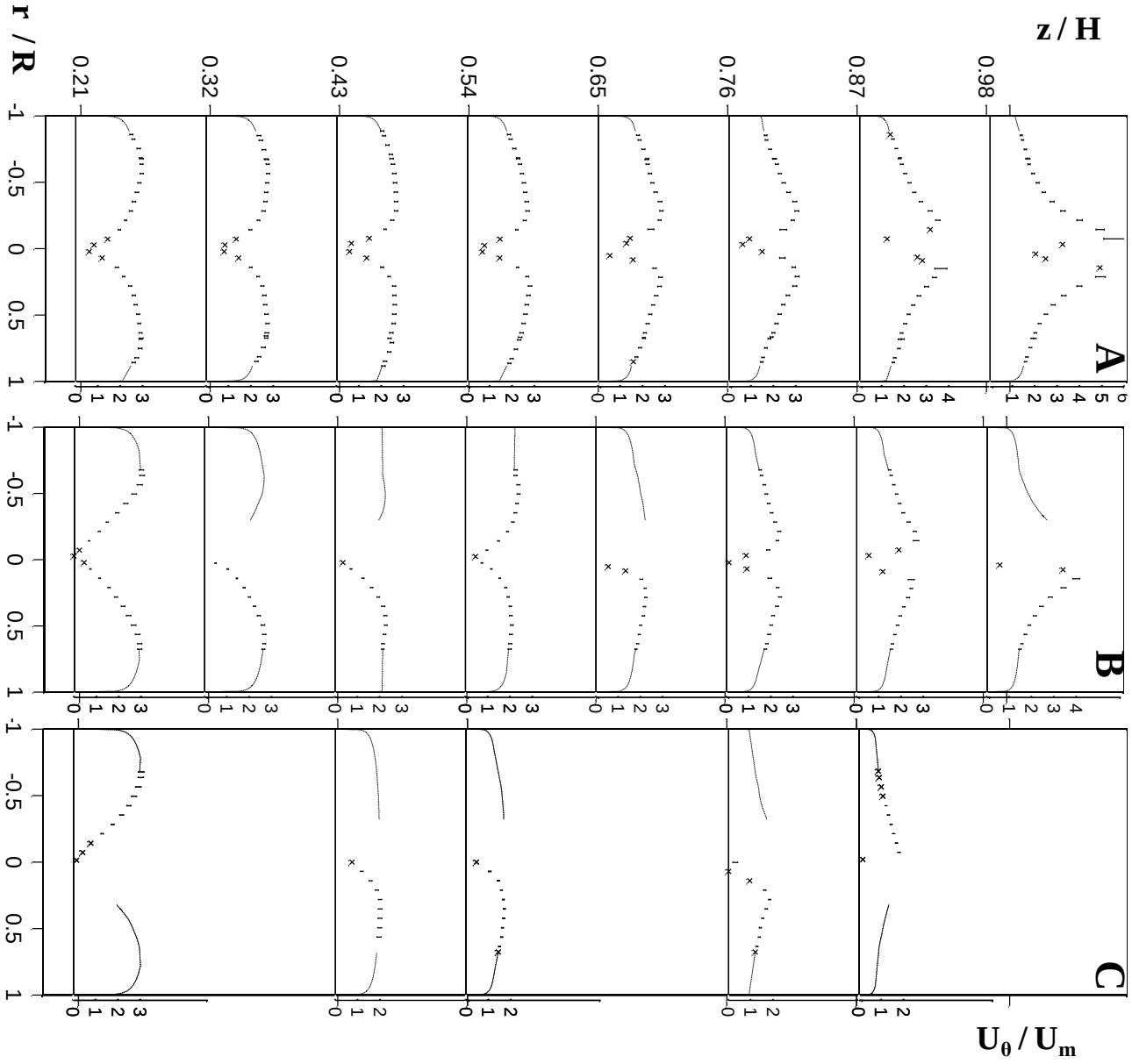

Figure 5: Scale I. Top to bottom case A, B & C. Tangential normalized velocity distributions. Re III. Left to right give the measurements at different axial positions, H x 0.21; 0.32; 0.43; 0.54; 0.65; 0.76; 0.87; 0.98. Bars indicate the maximum error.

Tangential velocity profiles in swirling flows are often characterized by studying the radial location of the maximum swirl. This divides the vortex in core, annular and transition zones (Yajnik & Aubbaiah 1973). A comparison of the data to the ideal velocity profile of a Rankine vortex illustrates how the measured field deviates from a system composed by a core zone where an inner force vortex leads to the linear increase in tangential velocity followed by an annular region where a free vortex shows exponential swirl decay.

In a relatively clean tower, case A, at the bottom end the tangential velocities peak at around 0.70 *R* and show a very wide transition zone, starting from approximately 0.10-0.15 *R*. As the location of maximum swirl is brought inwards downstream, the annular zone increases significantly. At the upper levels the transition region has been reduced to a section between around 0.10-0.20 *R* and both the core and annular zones are seen to describe closely the patterns of a force and a free vortex. The radius of the core region remains fairly constant along the axis, around 0.10-0.15 *R*.

The is in contrast with cases B & C which show a core section that extends beyond 0.40 *R* at the tower bottom end. As the vortex rises in the unit, the annular zone then starts to increase gradually, shifting the point of maximum swirl towards the centre. In case B, above 0.54 *H* a sharp change narrows this transition, which then goes from 0.10-0.30 *R* at 0.65 H down to 0.10-0.15 *R* at the top. In case B, a similar exponential decrease is observed in the annular zone at the top, although the magnitude of the tangential velocity is considerably lower than in case A.

In case C, the sharp change occurs between 0.21 and 0.43 *H*, after which the annular region increases gradually until covering the entire range above 0.10 *R* at 0.87 *H*. A transition from an exponential decrease towards a solid body rotation is also seen. Again, tangential velocity at the top decreases dramatically when compared to cases B & C

Figure 6 shows the evolution of the axial velocity profile. At the bottom, the mass flow concentrates close to the wall.

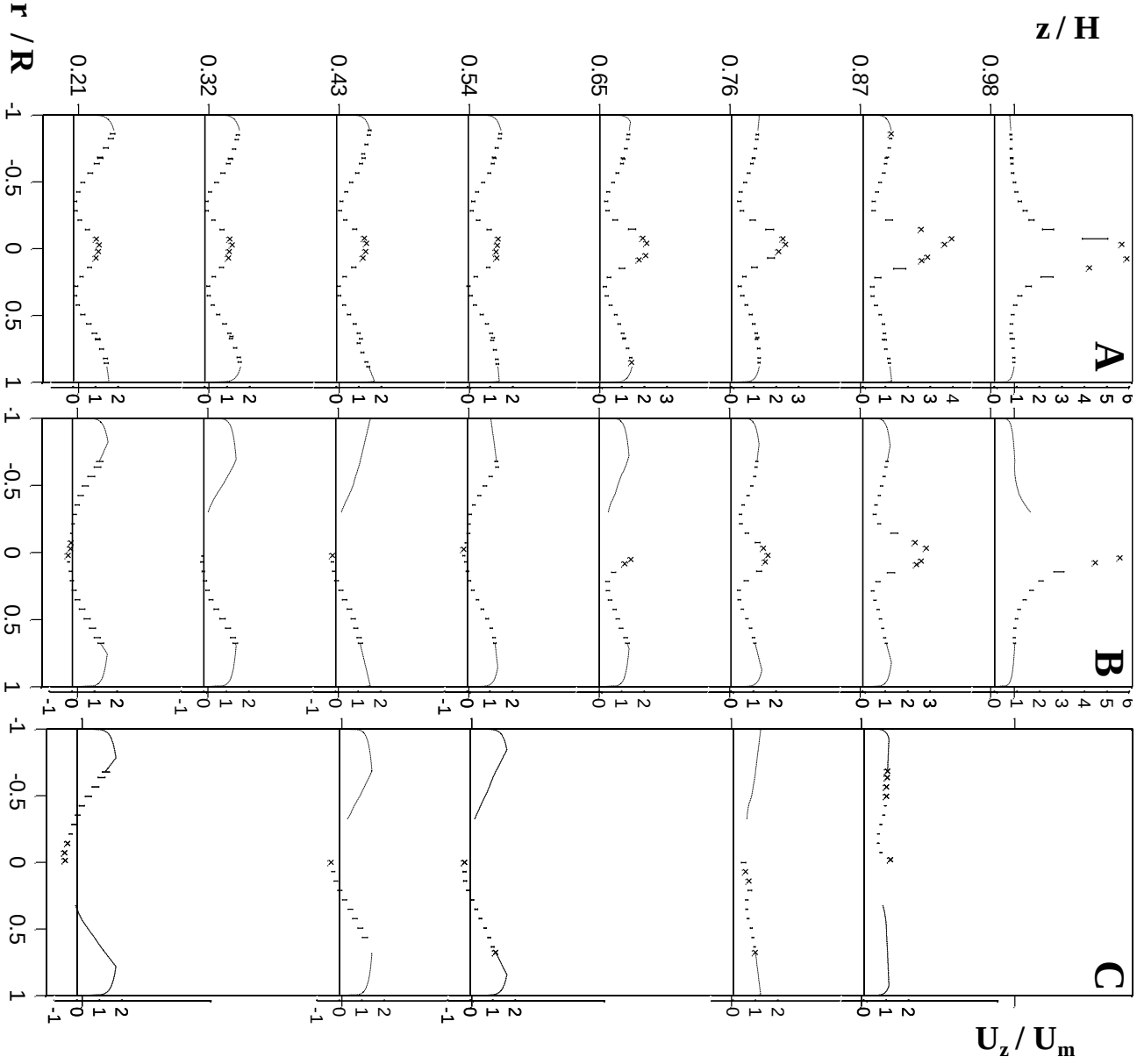

Figure 6: Scale I. Top to bottom case A, B & C. Axial normalized velocity distributions. Re III. Left to right give the measurements at different axial positions, H x 0.21; 0.32; 0.43; 0.54; 0.65; 0.76; 0.87; 0.98. Bars indicate the maximum error.

In case A, the maximum velocity is seen above 0.88 *R* and decreases at all levels as the vortex moves downstream. A second maximum is also appreciated at the centre. The inflexion point created varies gradually from around 0.35 to 0.30 *R* from bottom to top ends. The magnitude of the maximum increases gradually up to 0.65 *H* after which it begins to rise rapidly as the vortex approaches the top exit.

Remarkable differences are also appreciated when comparing the axial profiles for different deposition states. In cases B & C a reversion in the axial flow appears at the bottom core region. The extent of the negative flow observed diminished as the vortex rises until it reverts back, between 0.54-0.65 *H* in case B. After this point, a central maximum is formed and the velocity increases as we approach the exit, bringing the inflexion point from 0.25 *R* at 0.65 *H* up to 0.30 *R* at the top end. In case C, the extent of the negative flow increases significantly and once the flow reverts back between 0.54-0.76 *H* the axial maximum is not generated at the very centre, but at 0.15-0.20 *R*. It then moves inwards to the centre and at 0.87 *H* shows an inflexion point between 0.15-0.20 *R*. The magnitude of the maximum decreases significantly from A to B to C

In a free developing flow, axial velocity profiles are known to be dependent on swirl intensity and *Re*. An axial reversion in the flow occurs at central regions in cases where low pressure is created at the core by the centrifugal motion. As the swirl decays downstream, the extent of the negative flow diminish (Steenberg & Voskamp 1998, Chang & Dhir 1994). This may be altered in compressibility conditions where more complex recirculation patterns arise from the use of tangential inlets (Guo et al 2009). In such cases, a vortex breakdown can responsible for the axial reversion extending downstream.

The velocity patterns described for case A are in qualitative agreement with those obtained from experiments and simulations of a range of pilot scale counter current spray drying towers assuming smooth wall conditions (Bayly et al 2004, Harvie et al 2001). However a strong decrease in the magnitude of the tangential velocities is appreciated.

Notice that these patterns cannot be explained exclusively as a result of the decay of the swirling flow. The bottom end of the cylinder shows similar magnitudes for the tangential velocities that will generate in all cases a high centrifugal force, and yet the axial flow developed is clearly different. Further on, as it will be described later, the entire bottom section up to 0.54 *H* for cases A & B presents a similar swirl intensity, but one shows a flow reversion and the other does not. It is also noticeable that the inflexion point of the axial velocity profile relates to the dimensions of the exit conduct, or vortex finder, inserted at the top end, which appears to contain the force-vortex-type core described by the tangential velocity profiles.

This suggests that two differentiate regions are generated in case A, a core vortex that flows into the exit conduct and a outer vortex that moves up to the dead regions above. As this happens, the outer vortex rises and decays in intensity due to the friction caused by the wall. It feeds a radial mass inflow into the core zone and develops into a free vortex as it approaches the level of the vortex finder.

Due to the exit contraction, there is an obvious influence of the downstream conditions from the tower top into the development of the vortex, as expected from previous works (Luca-Negro & O'Doherty 2001) at least in case A. It appears that the level of recirculation in the tower is very much linked to the balance between the initial swirl intensity and the extent of the decay experienced though the unit, where cases A, B & C show an evolution from higher to a lower impact of the downstream conditions.

It is also worth noticing that the field shows consistent asymmetries, appreciated in an unbalance radial flow, which are particularly acute close to the exit. For case A, the asymmetries seems to increase for high *Re* numbers resulting in unbalanced mass flow rates from opposite sides of the axis. Asymmetry however seems to be closely related to deposition. It is particularly relevant in case B, where the tangential velocity above 0.54 *H*, preceding the reversion, show increasing values above 0.60 *R* in one side only, resulting in a strong gradient along the tangential direction.

Swirl decay

Impact of wall deposits

Figure 7 shows the axial evolution of Ω_o for scale I from which several conclusions can be drawn.

Very significant swirl decay occurs in counter current swirl spray drying towers. Case A restricts wall deposits to the minimum realistically possible in real operation, and yet it shows a reduction in Ω_o above 50% along the cylindrical section. The impact of Re in the vortex development was assessed by conducting measurements covering a range between 8×10^4 to 18×10^4. Similar trends are observed for case A. In fact, despite local differences between the normalized velocity profiles, they often lay within the experimental range of uncertainty. The vortex shape is found close to a self-impating system, that is, while velocity at each point is function of the overall bulk flow, the direction remains fairly independent. This falls in line with other experimental works (Hassall 2011) in the same units.

The presence of bands and patches of deposits in cases B & C accelerates the swirl decay. In spite of the large uncertainty owed to the extrapolation, comparing the rate of the decay of Ω_o within the different build up sections described in Table 2 demonstrates a clear correlation between the shear stress produced by different wall conditions and the rate of change of Ω.

A significant loss of angular momentum occurs in both cases within the spray projection region, 5.7-7.1 *D* for case B and 2.4-5.7 *D* for case C. It can be appreciated in figures 3 & 4 that those sections present deposits which are more concentrated and show a larger range of thicknesses. Figure 3 illustrates how the flow is forced to overcome the steps between the patches of deposits onto the bands, and then within the roughness height characteristic of each section.

It is uncertain how obstructions such as those shown in

figures 3 & 4 can relate to the roughness heights, $\Delta x/D$, used in available models for the flow over rough walls. Reality however dictate that deposits in real units will be spatially distributed, shifting from regions of clean walls to sections where uneven patches develop and stepping into bands of homogeneous thickness and possibly roughness height. In fact, in some scenarios, certain regions can show deposits that would not only disturb the structure of the turbulent boundary layer but acquire dimensions large enough to represent an obstruction to the convective flow. That might be the case of the initial drop seen in case C, which is believed to arise from a large range of thicknesses observed in the deposits. Case C also shows higher initial Ω, perhaps as the result of being subjected to a lower friction during the generation of the swirling motion in the cone.

In spite of such complexity, it is undeniable that deposits as those shown in figure 3 introduce a significant impact in the wall shear stress and in its relation with the Ω decay.

Figure 8 shows the decay of Ω_o versus the axial position in the cylinder, normalized versus the unit diameter in line with the evolution of the tangential shear stress in (4) and also over the total length between the air inlets and the vortex finder, H. It includes the evolution of Ω_o of all scales

Wall tangential shear stress is expected to be not just proportional but itself a function of swirl intensity. As a result, integration of (4) only yields an exponential decay for cases where high order terms may be neglected. For comparison purposes however, figure 8 includes the fitting of the decay curve of the homogeneous section of case A $z < 7.1\ D$, to a piecewise linear dependency between shear stress and swirl intensity as proposed by Kioth (1991).

Notice that in a confined unit the impact that Ω or Re may have in the evolution of velocity profiles, hence the streamline directions close to the wall, does not in principle relate to that of a free developing vortex. The exact dependency between Ω and the resulting decay rate curve of angular momentum owes to the variations introduced to pressure and velocity profiles, and is a priori, unknown. As described before, Ω impacts the vortex development substantially due to the effect in the pressure field and the generation of recirculation patterns.

As expected, wall shear stress and therefore the decay rate in figure 8 vary axially due to the spatial distribution of deposits. Abrupt changes in the rate of decay correlate with the presence of thick build up bands and regions of clean walls. The rate of decay observed at the bottom region for cases A & B is very similar where the coverage and distribution of deposits is limited. After 7.1 D however a thick band of build up arises in case B, product of the operation of nozzle/s above. A clear increase in the decay rate follows. Then it moderates in both cases to yield almost stable values at the upper end of the unit, where no deposits are observed at the wall in figure 3.

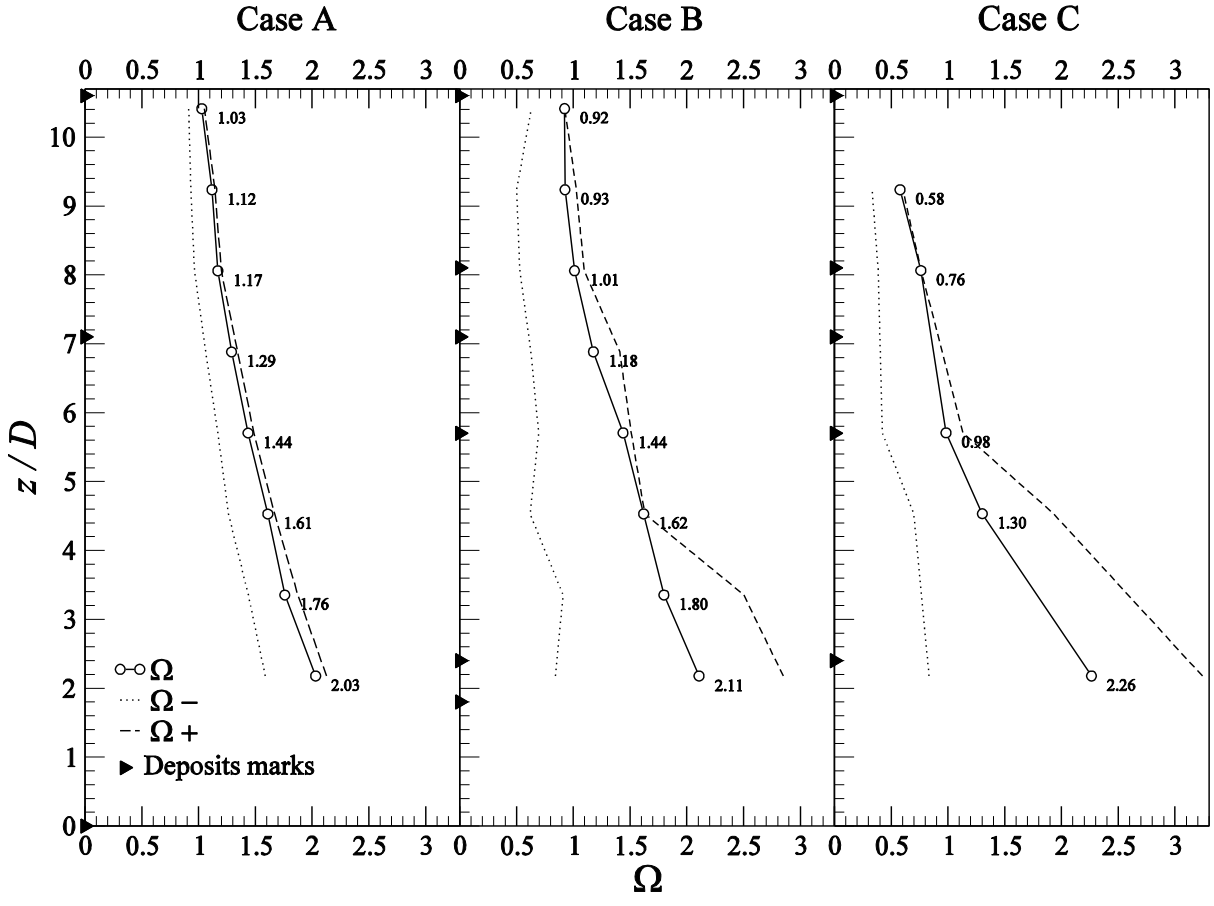

Figure 7: Swirl intensity estimates, Ω_o, at different axial positions for scale I. Left to right cases A, B & C. The location of build up sections defined in table 2 are marked in the abscissas.

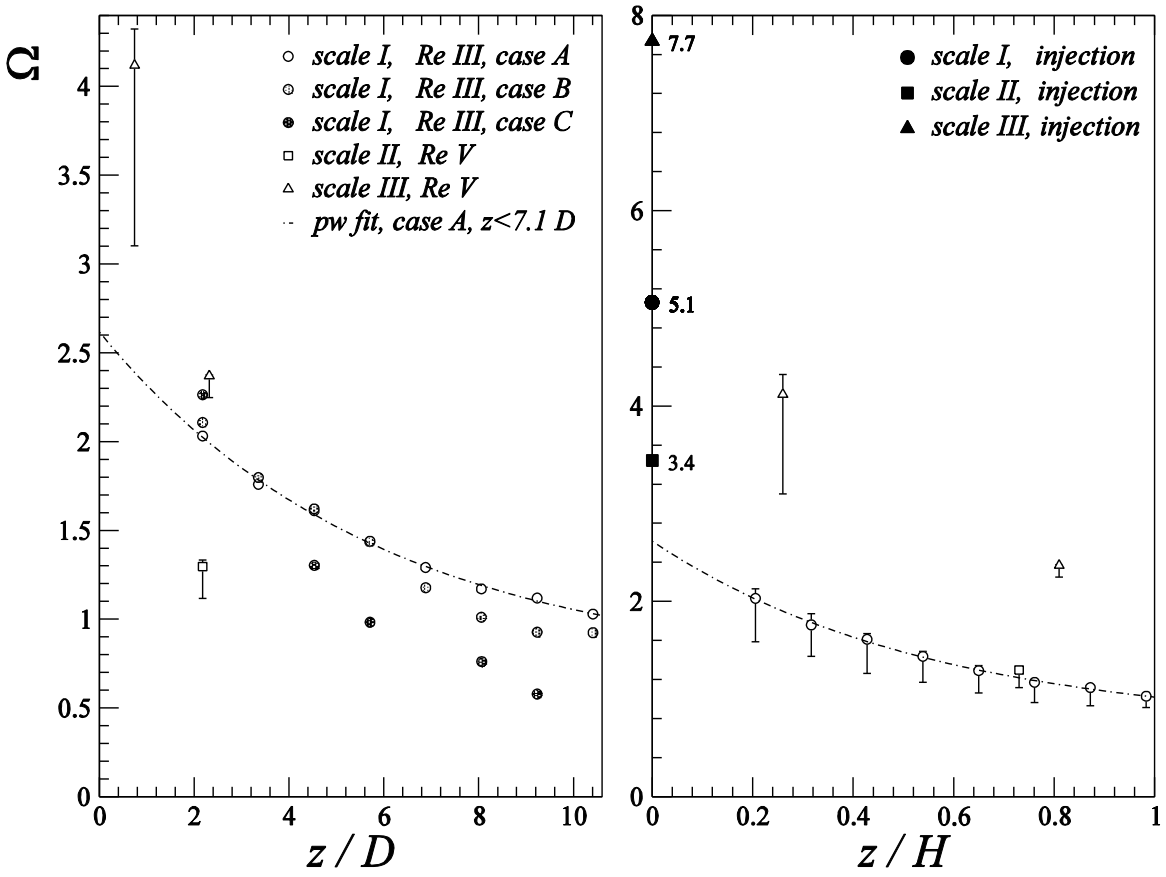

Figure 8: Swirl decay curves for Ω_0 in scales I, II & III. Left to right, axial distance in relation to the cylinder diameter or to the distance between the air inlets and the vortex finder. Error bars indicate the range Ω_- to Ω_+. Not included in left for clarity

The same trends arise in case C. The decay rate here is however far more pronounced at the bottom end and then reduces after surpassing the spray region. It increases again for the upper part where a final band of deposits is seen to reappear in figure 3. Once more, the sharp changes observed in the deposit thickness for case C seem to play an important role in the rate of loss of angular momentum.

Impact of tower geometry and scale.

Long cylinders such as pipes allow for the swirling flow to develop freely. Radial flows and axial recirculation respond to pressure differences caused by the centrifugal forces. In a large confined industrial unit such a cyclone or a counter-current swirl tower, the flow is constrained into a specific unit design. Its development is the result of a balance between the initial generation of swirl and the conduction towards the exit design.

The air leaves the confined space from a low pressure exit, centrally located at the top end. Within this conduit, a vortex finder is often inserted; see figure 1, it aims at stabilizing the flow and breaking the swirl motion further down the line, forcing the air through a series of straight channels. Position and diameter are known to be critical for the development of the pressure field.

Scale III produces higher swirl intensity in the cylinder, from 2.4 to 4, than scale I, from 1 to 2. Despite being operated at a high Reynolds, around 4.2 x 10^5, what is believed to reduce β in a free vortex flow over open pipes, it shows a higher decay rate, comparable to that obtained at the bottom region for case B, heavy deposits in scale I. However, the deposits morphology is unlikely to be the reason for this behavior. In the large scales deposits are evenly distributed and the relation to the diameter would be far from case C and more closely related to case A & B. This indicates that there is an effect other than surface roughness impacting the swirl decay rate, and might point to a stronger dependency of swirl intensity with the tangential wall shear stress than that reported in pipe flow.

Increases in both the initial swirl intensity and Reynolds are expected to provide competing effects in the swirl decay rate observed in force and free vortexes (Maddahian et al 2011). Now, let postulate which might be the impact that an increase of the operating Ω in a counter current swirl tower may bring to the overall development of the flow field, hence to the potential increase of the wall shear stress, by illustrating the examples given in scale I.

Pressure differences required for skewing the streamlines inwards in a high swirling flow increase with Ω, as higher centrifugal forces need to be overcome. Regions beyond the exit conduct in counter current towers are confined spaces and if a high swirling flow reaches them would respond to the accumulation of mass by recirculation and a pressure increase. In case C the low tangential velocities above 0.31 *H* allow the flow to be skewed inwards easily by low radial pressure gradients. As weak swirl reaches the top, the pressure build up beyond the exit is small. So it is the resulting velocity at the centre line, which owes to the

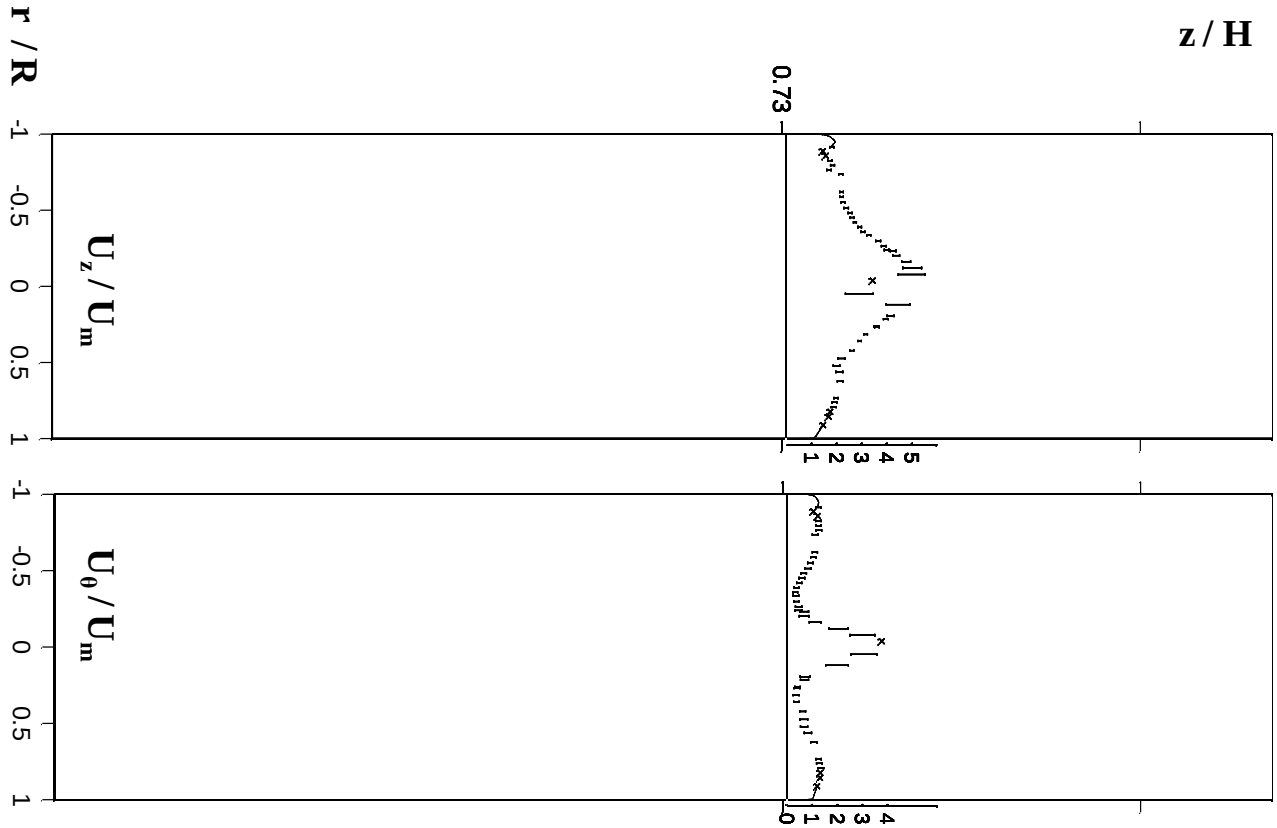

Figure 9: Scale II. Top to bottom. Axial and tangential normalized velocity distributions. Re V. Left to right give the measurements at different axial positions, H x 0.74. Bars indicate the maximum error.

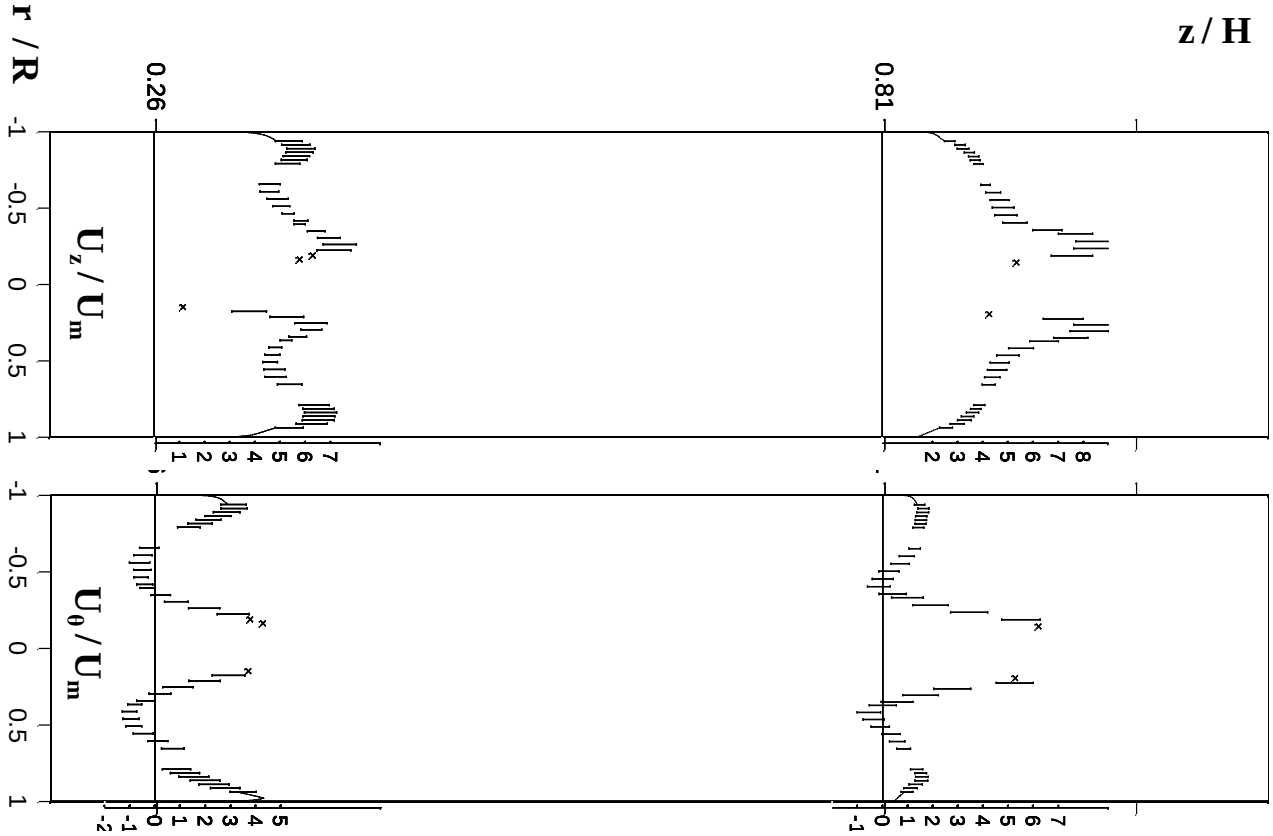

Figure 10: Scale III. Top to bottom. Axial and tangential normalized velocity distributions. Re V. Left to right give the measurements at different axial positions, H x 0.30, 0.93. Bars indicate the maximum error.

axial pressure gradient. The vortex bottom core, where the highest centrifugal forces still survive, can develop local low pressure regions as in a free developing vortex and result in the downwards reversion seen in figure 6.

For case B, as Ω at the top increases, so it does the angular momentum flux density in the annular zone. Pressure build up increases until what is required to make the pressure drop to the exit capable of skewing the vortex streamlines inwards. This can be observed in the variation inwards of the tangential velocity profiles at figure 5 from cases C to B to A. Higher pressure differences to the exit are generated and subsequently, the axial velocity at the centre increases to give the maximum described earlier. The annulus of minimum axial velocity created establishes a boundary between the force and free systems. The core zone is dominated by the pull from the top exit, while the annulus zone is dominated by the high swirling motion. Further on, as pressure builds up upstream, at a point at the centre the difference towards the exit rises – exit pressure is kept constant- but the differences towards the core below remain the same –rise in the same proportion- what results in the attenuation of the negative flow. Increasing Ω further in case A only strengthen these effects, rising the axial velocity maximum and preventing any negative flow from developing at the bottom end of the core.

The process outlined above is consistent with further measurements in the larger scales. Figures 9 & 10 present the axial and tangential velocities profiles of scales II & III Larger units that maintain a similar Ω at the top end, see scale II, still produces a comparable velocity profile despite having fairly different aspect ratios, operating *Re*, initial swirl intensity and swirl decay rate. On the contrary, scale III is operated at much higher initial and final Ω. The force required for conducting the vortex inwards raises and greater recirculation is now produced.

Qualitative differences can be seen between the velocity profiles in figures 5, 6 & 10. A full axial reversion of the flow is created that divides the outer zone into upwards and downwards sections. Notice that low pressure now is generated by much higher centrifugal forces at the bottom, both, at the injector level, Ω_i varying from 7.7 to 5.1, and surviving up to around 0.30 *H*, where Ω_o varies from 4.1 in scale III to 1.8 in scale I, case A. As a consequence, the axial reversion is exacerbated at the bottom end where a downwards flow region covers the range from 0.30-0.35 to 0.60-0.70 *R*. The inflexion point moves from 0.45-0.50 to 0.40 *R* as we rise in the unit, approaching the dimensions of the vortex finder. Tangential velocity profiles present now a strong minimum in the lower level with an inflexion point that situates between 0.50-0.65 *R* and moves inwards to 0.45 *R* at the top end. The outer section does not develop into a full free vortex and the exponential decay cease after 0.80 *R* where both tangential and axial velocities are seen to decrease rapidly towards the wall.

Conclusions

1-Particulate deposits have a strong influence in the development of an air vortex in industrial confined units.

2-The swirl intensity decay observed for a homogeneous distribution of a thin layer of detergent powder deposits appears to be consistent with the exponential decay reported for turbulent pipe flow, although the computed decay rates are up to one order of magnitude above.

3-The rate of decay is strongly correlated with the presence and the distribution of deposits. It increases drastically when the flow overcomes the deposit bands localized in the proximities of the operating nozzles. It also appears to present a dependency on the operating swirl intensity due to the effect that large values have in the velocity profiles.

4-A transition between different regimes seems to follow the swirl intensity surviving at the unit top end. Core and annular regions are clearly defined conducting the main flow inwards to the centrally located exit. High swirl intensities lead to the formation of a central axial velocity maximum persisting along most of the entire cylinder. Decreasing Ω leads to a regime where the bottom and top sections are dominated by the low pressures from the core bottom and the top exit respectively. The extent of the axial reversion zone becomes wider and higher in magnitude as the swirl intensity at the tower top decreases in scenarios of high friction. On the contrary, operating at higher swirl intensities, achieved for the largest units, exacerbate these effects and generate more pronounced downwards recirculation, creating a secondary annular reversed region.

The comments above introduce serious implications in the multi-phase modeling of swirling systems such as a spray driers or cyclones, where swirl decay is known to be responsible of a decrease in the collection efficiency (Hu et al 2004, Kaya et al 2011). However, the effect of wall friction upon the motion of the fluid phase is often disregarded in most numerical models dealing with swirling flows. And yet, failing to do so in the case of a counter-current spray drying tower as described here leads to unrealistic velocity profiles and the over prediction up to one order of magnitude of the carrier phase tangential velocity. Particle size in the production of detergent powder is fairly constant across scales and such differences have a determining impact in the predicted particle centrifugal inertia or the level of contact expected at the unit wall. In addition, the regimes mentioned in the axial velocity profiles would also affect both, the generation of re-entrained fines and the initial dispersion of the sprays, particularly when placed in regions of reverted flow.

In light of these observations, it becomes clear that design and numerical simulations of such units need to account for significant swirl decay in the carrier phase. The type and distribution of deposits formed during operation and cleaning also needs to be considered carefully as it has potential to cause a significant disruption to the vortex.

Potential remains to manipulate unit designs and accommodate the effects introduced by wall conditions. Ultimately, the initial swirl energy shall be optimized to enhance particle drying while avoiding excessive wall contact, in such manner that a degree of control is given over the particle deposition and aggregation processes.

Acknowledgements

VF is supported by an Engineering Doctorate Studentship sponsored by the Engineering and Physical Sciences Research Council (EPSRC) and Procter & Gamble in the Industrial Doctoral Centre in Formulation Engineering, School of Chemical Engineering, University of Birmingham

References

Bayly, A. E & Jukes, P & Groombridge, M & McNally, C . Airflow Patterns in a Counter-Current Spray Drying Tower - Simulation and Measurement. International drying symposium, Sao Paulo, 22-25 B, 775-781 (2004).

Chang, F & Dhir, V. K. Turbulent flow field in tangentially injected swirl flows in tubes. International journal of heat and fluid flow, Vol. 15, 346-356 (1994).

Cuerva, A & Sanchez-Andres, A. On sonic anemometer measurement theory. Journal of wind engineering and industrial aerodynamics, Vol. 88, 25-55 (2000).

Cuerva, A & Sanchez-Andres, & Navarro, J. On multiple-path sonic anemometer measurement theory. Experiments in fluids, Vol. 34, 345–357 (2003).

Cuerva, A & Sanchez-Andres, A & Lopez. O. Singularities and undefinitions in the calibration functions of sonic anemometers. Journal of atmospheric and oceanic technology, Vol. 21, 1868-1875 (2004).

Franchini, S & Sanchez-Andres, A & Cuerva, A. Measurement of velocity in rotational flows using ultrasonic anemometry: the flowmeter. Experiments in fluids, Vol. 42, 903- 911. (2007).

Franchini, S & Sanchez-Andres, A & Cuerva, A. Effect of the pulse trajectory on ultrasonic fluid velocity measurement. Experiments in fluids, Vol. 43, 969–978 (2007).

Guo, H.F & Chen, Z.Y & Yu, C.W. 3D numerical simulation of compressible swirling flow induced by means of tangential inlets. International Journal of Numerical methods in fluids, Vol. 59, 1285–1298 (2009).

Guo, B & Langrish, T.A.G & Fletcher. D.F. Simulation of turbulent swirl flow in an axisymmetric sudden expansion. AIAA journal, Vol. 39, 96–102 (2001).

Harvie, D.J.E & Langrish, T.A.G & Fletcher, D.F. Numerical simulations of the gas flow patterns within a tall form spray dryer. Trans IChemE, Vol. 79, 235-248 (2001).

Hassal, G. 2011. Wall build up in spray driers. EngD thesis. Chemical Engineering. University of Birmingham (2011).

Hu, L. Y & Zhou, L. X & Zhang, J. Studies on strongly swirling flows in the full space of a volute cyclone separator. AIChE Journal, Vol. 51, No. 3 (2005).

Jakirlic, S & Hanjalic, K & Tropea, C. Modelling rotating and swirling turbulent flows: A perpetual challenge. AIAA Journal, Vol. 40, 1984-1996 (2002).

Jimenez, J. Turbulent flow over rough walls. Annual Reviews in fluid mechanics, Vol. 36, 173-96 (2004).

Kaya, F & Karagoz, I & Avci, A. Effects of surface roughness on the performance of tangential inlet cyclone separators. Aerosol Science and Technology, Vol. 45, 988-995 (2011).

Kitoh, O. Experimental study of turbulent swirling flow in a straight pipe. Journal of fluid mechanics, Vol. 225, 445-479. (1991).

Kreith. F & Sonju, K. The decay of swirl in a pipe. Journal of fluid mechanics, vol. 22, 257-271 (1965).

Luca-Negro, O & O'Doherty, T. Vortex breakdown: a review. Progress in energy and combustion science, Vol. 27, 431-481 (2001).

Maddahian, R & Kebriaee, A & Farhanieh, B & Firoozabadi, B. Analytical investigation of boundary layer growth and swirl intensity decay rate in a pipe. Archives of applied mechanics, Vol. 81, 489-501 (2011).

Nakai, T & Shimoyama, K. Ultrasonic anemometer angle of attack errors under turbulent conditions. Agricultural and forest meteorology, Vol. 162-163, 14-26 (2011).

Probst. O & Cardenas. D. Review state of the art and trends in wind resource assessment. Energies, Vol. 3, 1087-1141 (2010).

Pruvost J & Legrand, J & Legentilhomme, P & Doubliez, L. Particle image velocimetry investigation of the 3D turbulent annular swirling decaying flow induced by means of a tangential inlet. Experiments in fluids, Vol. 29, 291-301 (2000).

Sommerfeld, M & Qui, H. Characterization of particle-laden, confined swirling flows by phase-doppler anemometry and numerical calculation. International journal of multi phase flow, Vol. 19, 1093-1127 (1993).

Steenbergen, W & Voskamp, J. The rate of decay of swirl in turbulent pipe flow. Flow Measurement and Instrumentation. Vol. 9, 67–78 (1998).

Walker, I. J. Physical and logistical considerations of using ultrasonic anemometers in aeolian sediment transport research. Geomorphology, Vol. 68, 57–76 (2005)

Wilczaki, J. M & Oncley, A.P & Stage S. A. Sonic anemometer tilt correction algorithms. Boundary layer meteorology, Vol, 99, 127–150 (2001).

Yajnik, K.S & Aubbaiah, V. Journal of fluid mechanics. Experiments on swirling turbulent flows. Part 1.Similarity in swirling flows. Vol. 60, 665-687 (1973)

Zhou, L. X & Li, Y & Chen, T & Xu, Y. Studies on the

effect of swirl numbers on strongly swirling turbulent gas-particle flows using a phase-Doppler particle anemometer. Powder Technology, Vol. 112, 79–86 (2000)